Theory of Resonant Rayleigh Scattering from Semiconductor Microcavities: Signatures of Disorder

Andrei V. Shchegrov

Rochester Theory Center for Optical Science and Engineering and Department of Physics and Astronomy, University of Rochester, Rochester, New York 14627-0171

Jacqueline Bloch,* Dan Birkedal,† and Jagdeep Shah

Bell Laboratories, Lucent Technologies, 101 Crawfords Corner Road, Holmdel, New Jersey 07733

(Received 5 November 1999)

We develop a self-consistent, microscopic theory of coherent resonant secondary emission from semiconductor microcavities in the normal-mode-coupling regime. Our theory provides a quantitative description of the *spectral*, *temporal*, and *angular* properties of the disorder-induced emission component—resonant Rayleigh scattering—and offers an intuitive physical explanation of emission properties.

PACS numbers: 78.66.–w, 73.20.Dx, 78.35.+c, 78.47.+p

The optical properties of semiconductor microcavities (MC), consisting of quantum wells (QW) embedded in an optical cavity, are strongly influenced by static disorder [1–9]. Many experimental [1,5] and theoretical [2–4] papers studied disorder-induced effects in the dynamics and the spectra of the specular component of MC emission due to resonant excitation. While the specular emission is modified by disorder, resonant Rayleigh scattering (RRS), the coherent component of the secondary (nonspecular) emission, exists *solely* due to disorder. Experimental means to probe disorder signatures directly, by isolating the RRS from incoherent luminescence, have been developed only recently [10,11].

First experiments on the MC RRS [7–9] showed that no adequate theory is currently available. So far, experimental analysis [7] had to rely on a phenomenological extension of the QW RRS theory [12]. However, such an extension cannot provide insight into MC RRS physics since the perturbative treatment of exciton-photon interaction [12,13] employed in the QW RRS theory is inapplicable to the normal-mode coupling regime of MC. Therefore, it remains unclear how the strong, nonperturbative exciton-photon interaction modifies the RRS emission pattern for MC as compared to that for QW. Only a rigorous, quantitative MC RRS theory can clarify this issue and answer important questions, which are now understood for QW RRS: how the interplay between inhomogeneous and homogeneous broadening mechanisms influences the RRS emission pattern, what determines the rise and decay behavior of the ultrafast RRS dynamics, etc. Development of such a theory requires an innovative theoretical effort since one has to abandon not only the simple perturbation theory, but also assumptions of in-plane momentum conservation or 1D character of disorder, which can greatly simplify the theory of MC specular emission [2,3].

In this Letter, we develop a novel, microscopic theory of MC RRS using a powerful many-body language that relies on propagators renormalized by both exciton-photon and exciton-disorder interactions. This formulation is self-consistent and allows expanding the RRS field and intensity in terms of the orders of polariton scattering, with the lowest order playing a dominant role. This theory makes an important step forward by providing a comprehensive *quantitative* description of the *angular, spectral,* and *temporal* properties of MC RRS. The theory also incorporates existing results [3,4] for the reflectivity (specular emission) spectra. Furthermore, the theory offers a qualitative filter picture of the MC RRS process. This picture predicts and explains drastic differences in the properties of RRS for MC and for QW—in particular a "ring" pattern in the angular distribution of MC RRS emission [9]. We also use our theory to go beyond the currently limited experimental knowledge [7–9] and (i) demonstrate the existence of different regimes for MC RRS determined by the relative magnitude of the inhomogeneous broadening of the QW exciton and the homogeneous broadening of the cavity photon, and (ii) analyze what determines the rise and decay of the ultrafast MC RRS dynamics. We expect the theory to stimulate further experimental effort and lead to a deeper insight into the optical properties of MC.

In the following, we consider RRS from a strongly coupled exciton-photon MC system as studied experimentally in Refs. [7,9] and model it by the Hamiltonian [3]:

$$H = \sum_{\mathbf{k}} (\hbar\omega_{\mathbf{k}} - i\gamma_p) a_{\mathbf{k}}^{\dagger} a_{\mathbf{k}} + \sum_{\mathbf{k}} (\hbar\Omega_{\mathbf{k}} - i\gamma_x) b_{\mathbf{k}}^{\dagger} b_{\mathbf{k}} + \sum_{\mathbf{k}} \hbar C_{\mathbf{k}} (a_{\mathbf{k}}^{\dagger} b_{\mathbf{k}} + a_{\mathbf{k}} b_{\mathbf{k}}^{\dagger}) + \sum_{\mathbf{k},\mathbf{k}'} V_{\mathbf{k}-\mathbf{k}'} b_{\mathbf{k}}^{\dagger} b_{\mathbf{k}'} , \quad (1)$$

where $\mathbf{k}$ is the in-plane momentum, $a_{\mathbf{k}}$ and $b_{\mathbf{k}}$ are the photon and exciton Bose operators, respectively, and $C_{\mathbf{k}}$ is the exciton-photon coupling constant. The cavity photon resonance $\hbar\omega_{\mathbf{k}} = \hbar\sqrt{\omega_0^2 + c_{\mathrm{cav}}^2 \mathbf{k}^2}$, where c_{cav} is the speed of light in the MC, is subject to homogeneous broadening

 0031-9007/00/84(15)/3478(4)$15.00

γ_p due to escape through the mirrors. A small homogeneous broadening γ_x of the exciton resonance $\hbar\Omega_{\mathbf{k}} = \hbar\Omega_0 + \hbar^2\mathbf{k}^2/2m_x$ is included in addition to the disorder that causes a dominating inhomogeneous broadening. The detuning of the cavity photon resonance relative to that of the exciton at wave vector $\mathbf{k}$ is defined by $\delta_{\mathbf{k}} = \hbar\omega_{\mathbf{k}} - \hbar\Omega_{\mathbf{k}}$. The Fourier coefficient $V_{\mathbf{k}}$ corresponds to the 2D disorder potential $V(\boldsymbol{\rho})$ that depends on the position vector $\boldsymbol{\rho} = (x, y)$ in the QW plane and acts on the exciton center-of-mass motion. We model $V(\boldsymbol{\rho})$ by a zero-mean, Gaussian random process, characterized by the correlation function $\langle V(\boldsymbol{\rho})V(\boldsymbol{\rho}')\rangle = g(|\boldsymbol{\rho} - \boldsymbol{\rho}'|)$, where the angle brackets denote an average over the ensemble of realizations of disorder, and assume $g(\rho) = V_0^2 \exp(-\rho/a)$ [13], where V_0 is the rms amplitude of the potential (inhomogeneous broadening) and a is its correlation length. As in previously used models [3,4,6], we assume that QW disorder felt by excitons is considerably more important than disorder in MC resonator(s) felt by cavity photons, therefore we disregard the inhomogeneous broadening of cavity photons.

The coherent emission following the optical excitation of the cavity at frequency ω is determined by the photon propagator $D^{\omega}_{\mathbf{k},\mathbf{k}'}$. It follows from Eq. (1) that it obeys the Dyson equation complemented by the Dyson equation for the exciton propagator $G^{\omega}_{\mathbf{k},\mathbf{k}'}$ [3]:

$$D^{\omega}_{\mathbf{k},\mathbf{k}'} = D^{\omega(0)}_{\mathbf{k}}\delta_{\mathbf{k},\mathbf{k}'} + \sum_{\mathbf{k}''} D^{\omega(0)}_{\mathbf{k}} C^{*}_{\mathbf{k}} G^{\omega}_{\mathbf{k},\mathbf{k}''} C_{\mathbf{k}''} D^{\omega}_{\mathbf{k}'',\mathbf{k}'}, \quad (2)$$

$$G^{\omega}_{\mathbf{k},\mathbf{k}'} = G^{\omega(0)}_{\mathbf{k}}\delta_{\mathbf{k},\mathbf{k}'} + \sum_{\mathbf{k}''} G^{\omega(0)}_{\mathbf{k}} V_{\mathbf{k}-\mathbf{k}''} G^{\omega}_{\mathbf{k}'',\mathbf{k}'}, \quad (3)$$

where $D^{\omega(0)}_{\mathbf{k}} = (\hbar\omega - \hbar\omega_{\mathbf{k}} + i\gamma_p)^{-1}$ and $G^{\omega(0)}_{\mathbf{k}} = (\hbar\omega - \hbar\Omega_{\mathbf{k}} + i\gamma_x)^{-1}$. The nonlocal, *resonant* interaction term $C^{*}_{\mathbf{k}} G^{\omega}_{\mathbf{k},\mathbf{k}''} C_{\mathbf{k}''}$ in Eq. (2) affects the evolution of a cavity photon between its excitation and escape through the mirrors in two important ways: (i) the photon and the exciton couple into MC eigenstates—polaritons; (ii) photon momentum can change ($\mathbf{k} \neq \mathbf{k}'$) due to coupling to excitons, which can be scattered by disorder.

Previous studies [3–5] focused on calculating $\langle D^{\omega}_{\mathbf{k},\mathbf{k}'}\rangle$, which is nonzero only for $\mathbf{k} = \mathbf{k}'$ and whose squared modulus determines the spectrum of the specular emission. To provide a complete description of the spectral, temporal, and angular properties of the MC RRS, we need to perform a much more difficult calculation of the average two-particle photon propagator $\langle D^{\omega}_{\mathbf{k},\mathbf{k}'} D^{\omega'*}_{\mathbf{k},\mathbf{k}'}\rangle$. We calculate this quantity along the lines set by many-body theory [14], arriving at the expression

$$\langle D^{\omega}_{\mathbf{k},\mathbf{k}'} D^{\omega'*}_{\mathbf{k},\mathbf{k}'}\rangle = D^{\omega}_{\mathbf{k}} D^{\omega'*}_{\mathbf{k}'} + |D^{\omega}_{\mathbf{k}}|^2 \Lambda^{\omega,\omega'}_{\mathbf{k},\mathbf{k}'} |D^{\omega'}_{\mathbf{k}'}|^2, \quad (4)$$

where $D^{\omega}_{\mathbf{k}}$ is defined by $\langle D^{\omega}_{\mathbf{k},\mathbf{k}'}\rangle \equiv D^{\omega}_{\mathbf{k}}\delta_{\mathbf{k},\mathbf{k}'}$ and $\Lambda^{\omega,\omega'}_{\mathbf{k},\mathbf{k}'}$ is the reducible vertex function, describing the photon energy transport in the MC. The first term on the right-hand side (rhs) of Eq. (4) describes the specular component studied elsewhere and will not be considered further, while the second term describes the RRS. Despite the formal resemblance of the present treatment to that developed in the electronic transport theory [14], there are essential differences. The primary difference is the presence of excitonic resonant features in the vertex $\Lambda^{\omega,\omega'}_{\mathbf{k},\mathbf{k}'}$, which is the direct consequence of the resonant interaction term $C^{*}_{\mathbf{k}} G^{\omega}_{\mathbf{k},\mathbf{k}''} C_{\mathbf{k}''}$ in Eq. (2). Coupling of exciton and photon resonance poles *automatically* accounts for the MC eigenmodes—polaritons. Thus, Eq. (4) allows us to reformulate the scattering problem self-consistently, in terms of propagators renormalized by exciton-photon and exciton-disorder interactions and to describe the interaction of MC polaritons with disorder perturbatively, in terms of single-scattering, double-scattering, etc.

A tedious calculation of $\Lambda^{\omega,\omega'}_{\mathbf{k},\mathbf{k}'}$ by summing the infinite series of ladder and maximally crossed diagrams (describing diffusion and localization phenomena [14]) showed that for realistic cavity parameters the result can be very well described by the single-scattering approximation, given by the simplest single-line ladder diagram. This reflects a fact that the MC RRS emission is primarily formed due to a resonant polariton excitation through its photon part, disorder-induced momentum scattering through its exciton part, and escape back to the vacuum through the photon part, while all higher-order processes play a minor role. A similar conclusion about the dominance of polariton single scattering in MC for the specular reflection was reached in Ref. [4]. Therefore, we limit our further presentation to a self-consistent, single-scattering approximation, which furthermore provides a transparent physical picture of the MC RRS.

We first approximate the series for $\Lambda^{\omega,\omega'}_{\mathbf{k},\mathbf{k}'}$ by its leading term, related to the two-particle exciton propagator,

$$\Lambda^{\omega,\omega'}_{\mathbf{k},\mathbf{k}'} \cong |C_{\mathbf{k}} C_{\mathbf{k}'}|^2 (\langle G^{\omega}_{\mathbf{k},\mathbf{k}'} G^{\omega'*}_{\mathbf{k},\mathbf{k}'}\rangle - \langle G^{\omega}_{\mathbf{k},\mathbf{k}'}\rangle\langle G^{\omega'*}_{\mathbf{k},\mathbf{k}'}\rangle). \quad (5)$$

Here the expression in brackets describes the scattering of exciton from disorder, while the factor $|C_{\mathbf{k}} C_{\mathbf{k}'}|^2$ determines the exciton coupling to the initial and final photon states described by the functions $|D^{\omega}_{\mathbf{k}}|^2$ and $|D^{\omega'}_{\mathbf{k}'}|^2$ in Eq. (4). To calculate $D^{\omega}_{\mathbf{k}}$, we approximate $D^{\omega}_{\mathbf{k}'',\mathbf{k}'}$ in the rhs of Eq. (2) by its mean value, dominating the photon field in the cavity, take the average, and solve the resulting equation analytically obtaining

$$D^{\omega}_{\mathbf{k}} = \{[D^{\omega(0)}_{\mathbf{k}}]^{-1} - |C_{\mathbf{k}}|^2 G^{\omega}_{\mathbf{k}}\}^{-1}. \quad (6)$$

We will also need the disorder-averaged exciton propagator $\langle G^{\omega}_{\mathbf{k},\mathbf{k}'}\rangle \equiv G^{\omega}_{\mathbf{k}}\delta_{\mathbf{k},\mathbf{k}'}$, which will be calculated by the approach described in Ref. [15]. Finally, evaluating the second term on the rhs of Eq. (4) at $\omega = \omega'$ in the leading order in V_0^2, we obtain the frequency-resolved RRS intensity $I_{\mathbf{k},\mathbf{k}'}(\omega)$ due to ultrafast (impulsive) excitation,

$$I_{\mathbf{k},\mathbf{k}'}(\omega) = |D^{\omega}_{\mathbf{k}} C_{\mathbf{k}} G^{\omega}_{\mathbf{k}}|^2 g_{\mathbf{k}-\mathbf{k}'} |G^{\omega}_{\mathbf{k}'} C_{\mathbf{k}'} D^{\omega}_{\mathbf{k}'}|^2. \quad (7)$$

The structure of Eq. (7) means that a photon with momentum $\mathbf{k}$ and energy $\hbar\omega$ entering the MC passes through an

effective filter $|D_{\mathbf{k}}^{\omega}|^2$ and couples (through the $C_{\mathbf{k}}$ factor) to an exciton state described by the resonant function $G_{\mathbf{k}}^{\omega}$. A polariton state is excited in the MC, since *the poles of* $|D_{\mathbf{k}}^{\omega} C_{\mathbf{k}} G_{\mathbf{k}}^{\omega}|^2$ *are located at the polariton energies.* Scattering (described by $g_{\mathbf{k}-\mathbf{k}'}$) occurs through the exciton part of polariton and the emission process described by the factor $|G_{\mathbf{k}'}^{\omega} C_{\mathbf{k}'} D_{\mathbf{k}'}^{\omega}|^2$ is the reverse of the excitation process. All essential properties of the MC RRS can be understood using this filter picture and can even be compared to the bare QW case, noting that removing the cavity photon filters $|D_{\mathbf{k}}^{\omega}|^2$ and $|D_{\mathbf{k}'}^{\omega}|^2$ from Eq. (7) yields the RRS spectrum for a bare QW.

Equation (7) allows us to gain so far unavailable insight into the spectral and angular characteristics of the MC RRS. First, we find that the MC RRS strongly depends on the scattering angle. This is illustrated in Fig. 1. In calculations throughout the paper we use $k = 1.5 \times 10^4$ cm^{-1} (corresponding to an external angle of incidence of 11°), $\gamma_x = 0.05$ meV, $\hbar\Omega_0 = 1.46$ eV, $C_{\mathbf{k}} = 1.65$ meV, $a = 10$ nm, and $m_x = 0.5m_e$, and indicate the remaining parameters in the captions. The polariton dispersion (Fig. 1a) transfers the finite broadening in the energy space into a broadening in the momentum space. These broadenings are accounted for in Eq. (7) by the finite spectral widths of the input and the output filters. Thus, there exists a range of resonantly excited polaritons (within the dashed boxes) that participate in the RRS process and produce the two-polariton RRS spectrum (Fig. 1c) and the momentum- (or angular)-resolved RRS intensity, which is peaked at $k' = k$ (Fig. 1b). The azimuthal dependence, entering in Eq. (7) only through $g_{\mathbf{k}-\mathbf{k}'}$, is suppressed for typical parameters ensuring the inequality $|\mathbf{k} - \mathbf{k}'|a \ll 1$, hence the momentum-resolved RRS emission is seen as a uniform ring (Fig. 1d)—in stark contrast with QW RRS, uniform in both polar and azimuthal angular coordinates due to negligible exciton dispersion [16].

Second, Eq. (7) demonstrates the existence of different regimes for MC RRS, defined by the ratio of the inhomogeneous (V_0) and homogeneous (γ_p) broadenings. Figure 2 illustrates the dependence of spectrally resolved MC RRS intensity (due to impulsive excitation) on detuning in two opposite regimes: (a) $V_0 = 0.9$ meV and $\gamma_p = 0.4$ meV and (b) $V_0 = 0.4$ meV and $\gamma_p = 0.9$ meV. Both Figs. 2a and 2b display characteristic polaritonic anticrossing behavior. However, the maximum of RRS intensity is shifted towards the photonlike polariton branch when the exciton resonance is broader than the photon resonance (Fig. 2a) and towards the excitonlike polariton branch in the opposite case (Fig. 2b). Tuning the cavity from slightly negative to slightly positive detuning shifts the weight of the RRS from the lower polariton branch to the upper polariton branch (Fig. 2a) or vice versa (Fig. 2b), depending on the prevailing broadening mechanism. This balance between V_0 and γ_p also causes the maxima of RRS spectrally resolved intensity to appear not exactly at resonance ($\delta_{\mathbf{k}} = 0$), as one might expect, but at a slightly positive or negative detuning.

We next address another unsolved problem, that of calculating the time-resolved MC RRS intensity after an impulsive excitation. To reduce the high computational cost of this quantity, determined by $\langle |D_{\mathbf{k},\mathbf{k}'}(t)|^2 \rangle - |\langle D_{\mathbf{k},\mathbf{k}'}(t) \rangle|^2$, we neglect the exciton dispersion ($m_x \to \infty$) and obtain an explicit expression for the 2D inverse Fourier transform of $\Lambda_{\mathbf{k},\mathbf{k}'}^{\omega,\omega'}$ in Eq. (5):

$$\Lambda_{\mathbf{k},\mathbf{k}'}(t,t') \propto |C_{\mathbf{k}} C_{\mathbf{k}'}|^2 e^{i\Omega_0(t-t') - \gamma_x(t+t')} e^{-V_0^2(t^2+t'^2)/2} \times \int d^2\rho \, e^{i(\mathbf{k}-\mathbf{k}')\cdot\boldsymbol{\rho}} [e^{tt' g(\rho)} - 1]. \quad (8)$$

We tabulate this integral on a 1024×1024 grid of (t, t'), then take 2D fast Fourier transform, multiply the result for $\Lambda_{\mathbf{k},\mathbf{k}'}^{\omega,\omega'}$ by $|D_{\mathbf{k}}^{\omega}|^2 |D_{\mathbf{k}'}^{\omega'}|^2$, and obtain the RRS term in Eq. (4). The inverse 2D fast Fourier transform of this term yields the scattered photon field autocorrelation function $\langle \mathbf{E}^{(-)}(t) \cdot \mathbf{E}^{(+)}(t') \rangle$ identical to the time-resolved RRS

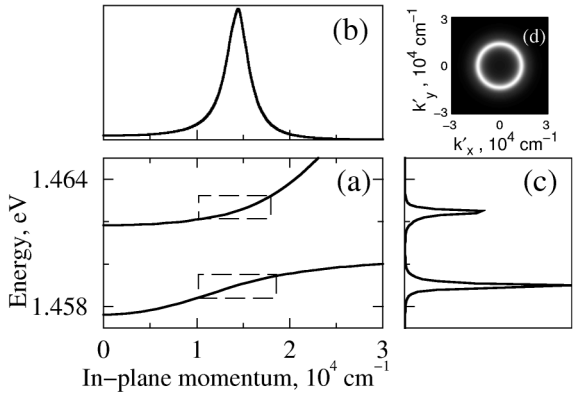

FIG. 1. (a) Microcavity polariton dispersion curves; (b) angularly integrated RRS spectrum; (c) spectrally integrated RRS intensity as a function of the in-plane momentum k' of the scattered photon; (d) spectrally integrated RRS intensity as a function of the components of $\mathbf{k}'$. Parameters used in the calculation are $\delta_{\mathbf{k}} = 0$, $V_0 = 0.5$ meV, $\gamma_p = 0.2$ meV. The areas within dashed rectangles in plot (a) show the polariton states participating in RRS.

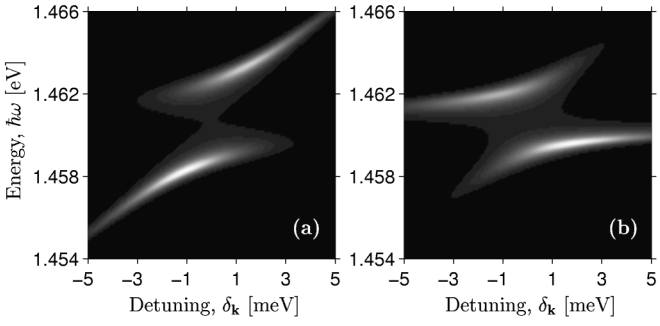

FIG. 2. Gray scale plots of the frequency-resolved RRS intensity vs detuning: (a) $V_0 = 0.9$ meV, $\gamma_p = 0.4$ meV, (b) $V_0 = 0.4$ meV, $\gamma_p = 0.9$ meV.

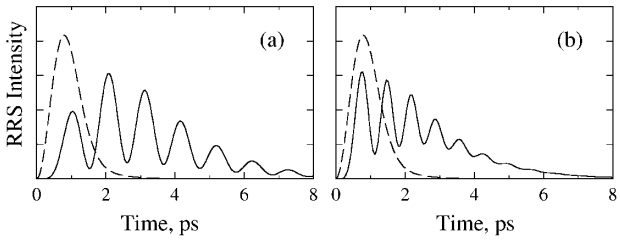

FIG. 3. RRS dynamics for $V_0 = 0.9$ meV, $\gamma_p = 0.4$ meV, and detunings of (a) $\delta_{\mathbf{k}} = 0$ and (b) $\delta_{\mathbf{k}} = 4$ meV. Solid lines: MC; dashed lines: bare QW. Vertical scaling of all curves is adjusted to make the comparison of their time scales easier.

intensity at $t = t'$. The described procedure amounts to calculating a fivefold integral, but, in fact, takes only a few seconds on a PC.

Using parameters of Fig. 2a we show in Fig. 3 MC RRS dynamics (solid lines) for two different cavity detunings and contrast these data with RRS dynamics for the bare QW (dashed lines), not embedded in a cavity. The beats seen in the MC RRS are due to the coherent excitation of both polariton branches, and the different beat periods are due to different polariton splitting for different detunings. While the QW RRS dynamics, given by Eq. (8) with $t = t'$, rises on the scale $t \sim \hbar/V_0$ [12], the MC RRS dynamics is determined by the effective polaritonic filters discussed above. At $\delta_{\mathbf{k}} = 0$ (Fig. 3a), both polaritons are spectrally narrow and have almost identical strength (see Fig. 2a). These two factors lead to the delayed rise (as compared to QW RRS) and large-amplitude beats in MC RRS, respectively. At $\delta_{\mathbf{k}} = 4$ meV (Fig. 3b) the lower polariton branch spectrally broadens and the upper polariton spectrally narrows. This results in an earlier rise of the MC RRS as observed experimentally [7]. The MC RRS at $\delta_{\mathbf{k}} = 4$ meV is primarily determined by the emission from the lower polariton branch at early times and the MC RRS emission maximum is seen to almost coincide with the QW RRS maximum. At later times ($t \sim 5$ ps) the emission is solely due to the narrower upper polariton branch, explaining the absence of beats at these times. Thus, the decay of beats in resonant secondary emission from MC is *not* sufficient to conclude the absence of RRS, because the response of the two polariton branches occurs on different time scales. We also note an enhancement of the MC RRS over the QW RRS at late times. It occurs due to the increased time (as compared to the QW) the coherent polarization "spends" in the MC before escaping to the vacuum. For long times the decay of the MC RRS (not shown) is essentially set by the decay of the QW RRS [13].

We conclude by pointing out the comprehensive nature of the newly developed theory of resonant Rayleigh scattering from semiconductor microcavities. This theory provides a quantitative description of the spectral, temporal, and angular characteristics of MC RRS. It also qualitatively explains the angular "ring" pattern of the MC RRS emission, and automatically accounts for polariton coherent features in RRS. In addition, the theory predicts different regimes for the MC RRS determined by the competition between inhomogeneous exciton and homogeneous photon broadenings—such a competition makes the MC RRS distinctly different from the QW RRS. Finally, the power of the many-body technique employed in this work can be naturally extended to other important problems, such as many-body nonlinear correlation phenomena in microcavities.

D. B. acknowledges financial support from the Danish Natural Sciences Research Council. A. V. S.'s research was supported by the Air Force Office of Scientific Research under Grant No. F49620-00-1-0125 and by the Engineering Research Program of the Office of Basic Energy Sciences at the Department of Energy under Grant No. DE-FG02-90ER 14119.

*Present address: Laboratoire de Microstructures et Microélectronique, CNRS, France.
†Present address: Research Center COM, Technical University of Denmark.

[1] C. Weisbuch *et al.*, Phys. Rev. Lett. **69**, 3314 (1992); T. B. Norris *et al.*, Phys. Rev. B **50**, 14 663 (1994); D. M. Whittaker *et al.*, Phys. Rev. Lett. **77**, 4792 (1996).
[2] V. Savona and C. Weisbuch, Phys. Rev. B **54**, 10 835 (1996).
[3] V. Savona *et al.*, Phys. Rev. Lett. **78**, 4470 (1997).
[4] D. M. Whittaker, Phys. Rev. Lett. **80**, 4791 (1998).
[5] C. Ell *et al.*, Phys. Rev. Lett. **80**, 4795 (1998).
[6] D. S. Citrin, Phys. Rev. B **54**, 16 425 (1996).
[7] G. R. Hayes *et al.*, Phys. Rev. B **58**, R10 175 (1998).
[8] M. Gurioli *et al.*, Phys. Rev. B **59**, R5316 (1999).
[9] T. Freixanet *et al.*, Phys. Rev. B **60**, R8509 (1999); J. Bloch *et al.*, in *Proceedings of the Quantum Electronics and Laser Science Conference, Baltimore, MD, 1999: QELS'99* (Optical Society of America, Washington, DC, 1999).
[10] D. Birkedal and J. Shah, Phys. Rev. Lett. **81**, 2372 (1998).
[11] W. Langbein, J. M. Hvam, and R. Zimmermann, Phys. Rev. Lett. **82**, 1040 (1999).
[12] R. Zimmermann, Nuovo Cimento Soc. Ital. Fis. **17D**, 1801 (1995).
[13] A. V. Shchegrov, D. Birkedal, and J. Shah, Phys. Rev. Lett. **83**, 1391 (1999).
[14] D. Vollhardt and P. Wölfle, Phys. Rev. B **22**, 4666 (1980).
[15] S. Glutsch and F. Bechstedt, Phys. Rev. B **50**, 7733 (1994).
[16] Note that we obtained the ring pattern by averaging the MC RRS intensity over the ensemble of disorder realizations. An experiment probing only a single realization of disorder is expected to find bright speckles within a ring, while for a QW such a speckle pattern is uniform [11,13].